Food Packaging and Shelf Life 56 (2026) 101808

Contents lists available at ScienceDirect

Food Packaging and Shelf Life

journal homepage: www.elsevier.com/locate/fpsl

A data-driven framework for remaining shelf-life prediction of sweet cherries under modified atmosphere packaging and variable cold-chain conditions

Smit Patel [a], Rishabh Goyal [a], Carolina A. Torres [b], Juming Tang [a], Kang Huang [a], Charles L. Munson [c], Shyam S. Sablani [a,*]

[a] Department of Biological Systems Engineering, Washington State University, Pullman, WA 99164-6120, United States
[b] Department of Horticulture, Tree Fruit Research & Extension Center, Washington State University, Wenatchee, WA 98801, United States
[c] Department of Finance and Management Science, Washington State University, Pullman, WA 99164-4746, United States

ARTICLE INFO

Keywords:
Remaining shelf-life (RSL)
Modified atmosphere packaging
Cold-chain variability
Sweet cherries
Deep learning
Shelf-life prediction
Postharvest quality

ABSTRACT

Accurate shelf-life prediction establishes a baseline under controlled storage, whereas remaining shelf-life (RSL) prediction enables informed decision-making in dynamic food systems. Sweet cherries stored under modified atmosphere packaging (MAP) experience quality degradation driven by the coupled effects of time, temperature, respiration, and gas composition. While shelf-life can be estimated under controlled storage, translating this information to dynamic cold-chain environments requires models that account for cumulative handling and temperature variability. Multiple regression, machine learning, and deep learning models were evaluated to estimate quality attributes, gas composition, and shelf-life under controlled storage conditions. Across all tested approaches, deep learning models consistently outperformed traditional methods. For shelf-life prediction, the one-dimensional convolutional neural network (1D-CNN) demonstrated the highest predictive accuracy (RMSE 1 day). To extend prediction beyond shelf-life, a unified framework was developed for RSL estimation by integrating physics-based respiration and gas exchange modeling with data-driven learning. A generative adversarial network was used to generate internally consistent quality state variables required for RSL estimation when direct measurements are unavailable. Under simulated moderate and extreme cold-chain abuse scenarios, the 1D-CNN achieved the lowest prediction error for RSL estimation, with a mean squared error on the order of 1 day, and captured stepwise and cumulative RSL losses associated with transient temperature excursions. The proposed framework enables time-resolved RSL prediction under realistic cold-chain conditions and provides a practical foundation for decision-support tools aimed at reducing postharvest losses, optimizing logistics, and improving quality management of perishable produce in applied food systems.

1. Introduction

Global food supply chains are complex systems shaped by logistics, environmental variability, market demand, and regulatory constraints. Unlike industrial supply chains, food systems must also account for biological variability and perishability, making postharvest management particularly challenging (Zhu et al., 2018). Fresh fruits and vegetables are especially vulnerable to postharvest losses due to limited shelf-life and sensitivity to handling and storage conditions, underscoring the need for improved strategies to preserve quality and reduce waste (Porter et al., 2016).

Shelf-life labeling for fresh produce is traditionally based on static estimates derived under ideal storage conditions. Such approaches fail to account for temperature fluctuations and handling stress encountered during real distribution, often leading to premature disposal of marketable product or unintended sale of compromised fruit. In response, data-driven and time-resolved modeling approaches that integrate real-time environmental information have gained attention as more responsive alternatives for shelf-life assessment (Chen et al., 2023; Shi et al., 2024).

Sweet cherries (*Prunus avium*), particularly high-value cultivars such as 'Bing', exemplify the challenges associated with managing highly perishable fruit. Cherry marketability is largely determined by visual

* Corresponding author.
E-mail address: ssablani@wsu.edu (S.S. Sablani).

https://doi.org/10.1016/j.fpsl.2026.101808
Received 29 January 2026; Received in revised form 24 June 2026; Accepted 2 July 2026

Nomenclatures

Symbols

R	Respiration rate (mL kg^{-1} hr^{-1})
T	Temperature (K)
t	Time (hr)
E_a	Activation energy (kJ mol^{-1})
V	Volume (mL)
U	Universal gas constant (0.082057 L atm mol^{-1} K^{-1} or 0.008314 kJ K^{-1})
w	Weight of product (kg)
P	Partial pressure (atm)
p	Transmission rate of the packaging material (mL cm^{-2} day^{-1} atm^{-1})
L	Headspace (mL)
A	Surface Area (cm^2)
Q	Quality parameter (fruit firmness, red hue and green hue)

Superscript and subscript

O_2	Oxygen
CO_2	Carbon dioxide
o	Environment outside of the package
i	Environment inside of the package
t	Current time stamp
$t-1$	Previous time stamp
ref	Parameter at $t-1$ time
r	Respiration
p	Packaging
thr	The endpoint of quality

and textural attributes, with color and firmness serving as primary indicators of consumer acceptance (Habib et al., 2017). While fruit size is standardized prior to packaging, color and firmness evolve dynamically in response to storage conditions and physiological processes. Temperature fluctuations, postharvest handling practices, and packaging environments strongly influence respiration rate, enzymatic activity, and biochemical degradation, making cold-chain integrity critical for maintaining quality (Shukla & Jharkharia, 2013).

Modified atmosphere packaging (MAP) is widely used to extend shelf-life by reducing oxygen and increasing carbon dioxide concentrations, thereby suppressing respiration and microbial growth (Sandhya, 2010). In cherries, reduced oxygen slows metabolic activity, while elevated carbon dioxide can delay spoilage and decay (Chaix et al., 2015; Joshi et al., 2019). However, MAP effectiveness is highly product-specific and depends strongly on packaging material permeability and external temperature conditions (Mangaraj & Goswami, 2011). As temperature increases, respiration accelerates, altering internal gas composition and influencing deterioration pathways, indicating that shelf-life behavior under MAP reflects coupled interactions among temperature history, respiration kinetics, and gas exchange.

Recent studies have explored dynamic and data-driven shelf-life modeling approaches that integrate physiological and environmental variables. Stochastic and kinetic models incorporating temperature dependence have shown improved predictive accuracy for several commodities (Chen et al., 2023; Torres-Sánchez et al., 2020; Tsironi et al., 2017). Advances in machine learning and deep learning have further enabled modeling of non-linear relationships between environmental conditions and quality evolution, with multivariate approaches outperforming static or univariate models (Cui et al., 2023). Neural network–based methods have demonstrated strong performance for -life prediction in fruits such as apples, strawberries, tomatoes, and mushrooms (Cao et al., 2021; Fu et al., 2019; Goyal et al., 2024; Qiao et al., 2022). For sweet cherries, temperature-dependent kinetic and physiological studies have shown that thermal fluctuations accelerate enzymatic pathways associated with pigment and cell wall degradation, directly affecting color and firmness (Xin et al., 2021; Xing et al., 2025a).

Despite these advances, many existing approaches remain limited in their ability to represent realistic cold-chain variability or to translate quality evolution into time-resolved usability metrics. Shelf-life prediction under controlled conditions provides useful baseline information but does not capture the evolving nature of product condition during distribution. Remaining shelf-life estimation, by contrast, reflects the time-dependent distance to a predefined quality threshold at intermediate points during storage and therefore requires models capable of accounting for cumulative and potentially irreversible effects of prior handling and temperature abuse.

The present study addresses this gap by developing and applying a data-driven framework for modeling quality evolution, shelf-life, and remaining shelf-life of Bing sweet cherries under modified atmosphere packaging. Controlled storage experiments were used to integrate temperature history, respiration-driven gas dynamics, and image-derived quality indicators within machine learning and deep learning architectures representative of commercial practices. The framework was subsequently applied under simulated cold-chain abuse scenarios to evaluate remaining shelf-life behavior under non-uniform temperature histories. This study integrates physiological understanding, modified atmosphere packaging behavior, and data-driven modeling to establish a unified framework for remaining shelf-life prediction of highly perishable produce under variable cold-chain conditions.

2. Materials and methods

2.1. Model development for quality, gas, and shelf-life kinetics

2.1.1. Cherry material and quality measurements

Sweet cherry (*Prunus avium*) was selected as the model horticultural product in this study due to its high commercial value**,** short postharvest shelf-life, and strong sensitivity to storage temperature and atmospheric conditions, which make it particularly suitable for evaluating shelf-life prediction frameworks under MAP. Among commercially cultivated sweet cherries, the cultivar 'Bing' was chosen because of its dominant market share, wide geographic distribution, and frequent use as a reference cultivar in postharvest and packaging studies, enabling comparison with existing literature.

Cherry quality attributes are product- and market-specific. For 'Bing' cherries, firmness and color are primary determinants of commercial acceptance and market value, as they strongly influence visual appeal and consumer perception (Habib et al., 2017). Fruit size, although an important quality attribute, is controlled during pre-packaging grading and remains largely unchanged during storage. Therefore, only fruit firmness and color were selected as quality indicators for model development.

Fruit firmness (FF, g mm^{-1}) was measured using a FirmTech Fruit Firmness Tester (BioWorks, Inc., USA). A circular disc probe was used to measure the force required to compress the fruit by 1 mm. FF was recorded for individual cherries, and replicate averages were used for subsequent analysis.

Cherry color was quantified using hue spectrum fingerprinting following Le Nguyen et al. (2020) and Nguyen et al. (2021). Images were captured using fixed camera settings (shutter speed 1/50 s, aperture f/5.6, ISO 100, white balance 4000 K). Hue angle (0–360°) was plotted against relative saturation (0–1). Pixels with saturation values below 0.05 were excluded to reduce low-saturation noise and avoid unstable hue values from nearly achromatic regions. This thresholding step was not used as the primary background-segmentation method. Images were acquired using a plain white and consistent background across all samples, minimizing background-related variation during hue-spectrum extraction. Images were acquired using grouped cherries as shown in Fig. 1, and hue-angle distributions were generated from all retained pixels. The minor peak observed near 100° hue angle corresponds primarily to stem tissues. Because these pixels represented a relatively small proportion of the total image area, their influence on the overall hue distribution and temporal color change analysis was limited.

2.1.2. Gas composition measurement

MAP was implemented using commercially available low-density polyethylene (LDPE) film with an average thickness of 33 μm. The packaging material was a proprietary LDPE with measured gas transmission rate values of 2.43–2.44 mL cm^{-2} day^{-1} atm^{-1} for CO_2 and 0.33 mL cm^{-2} day^{-1} atm^{-1} for O_2 measured at 23 °C and 90% relative humidity. Approximately 100 g of cherries of uniform size were sealed in LDPE pouches with absorbent pads. Initial headspace gas composition was assumed to be in equilibrium with ambient air (20.6% O_2, 0.0% CO_2). Internal gas composition was measured periodically using a Dansensor® Checkpoint 3 (MOCON Inc., Minneapolis, MN, USA) with an accuracy of ±0.1% for O_2 and CO_2 measurements.

2.1.3. Experimental design for model development

Packaged cherries were stored at 0, 4, 8, and 13 °C, representing typical cold-chain conditions and potential temperature fluctuations (Koutsimanis et al., 2015). Initial firmness and color measurements were collected prior to storage. Sampling frequency varied with temperature, with six sampling points collected over two days at 8 °C and 13 °C, and six sampling points collected over seven days at 0 °C and 4 °C. These data were used exclusively for model development and kinetic analysis. At each designated sampling interval, a set of three replicate packages was removed from storage and evaluated for gas composition without breaching the package. The packages were then opened for color

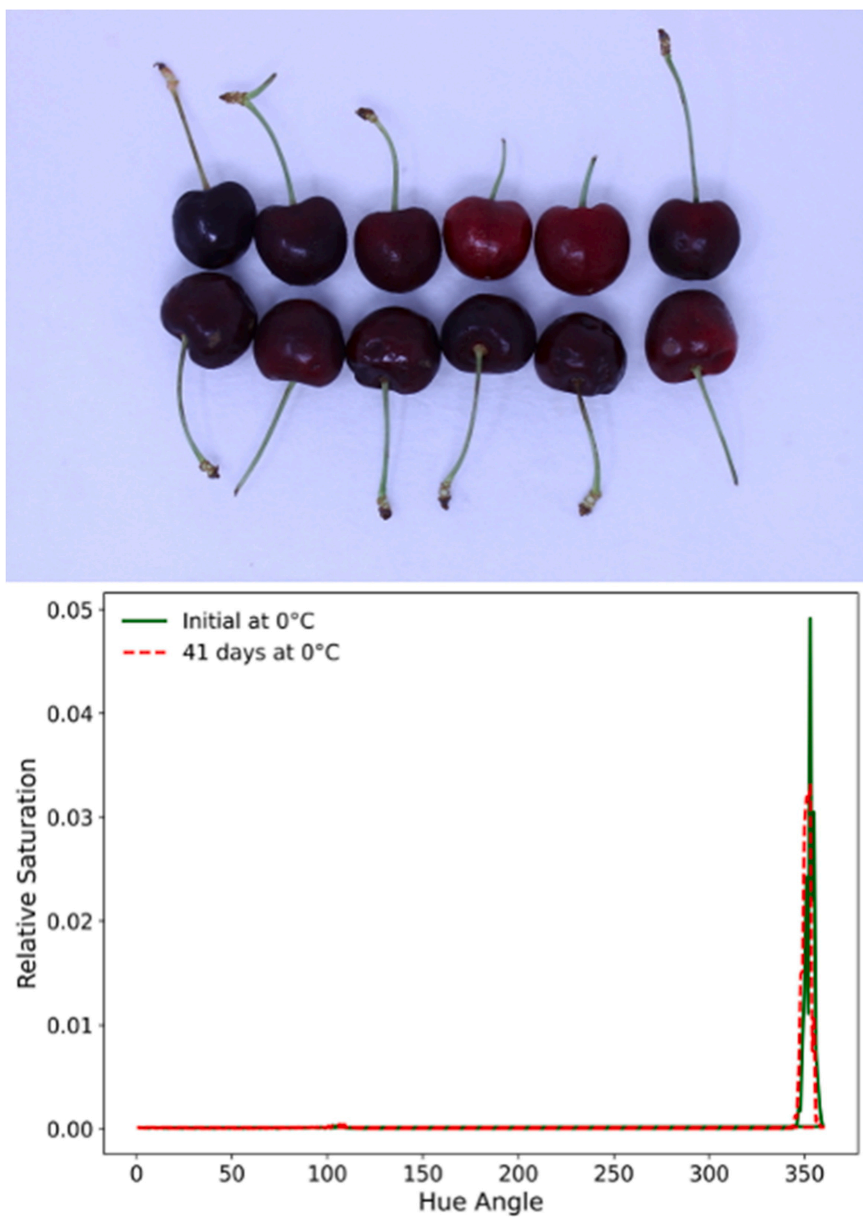

Fig. 1. Representative hue spectra of 'Bing' sweet cherries obtained using hue spectrum fingerprinting, illustrating changes in color distribution before storage and after 41 days of storage at 0 °C. Hue angle is plotted against relative saturation, with green and red regions corresponding to characteristic cherry surface and stem coloration.

imaging and firmness measurements. Since package access and firmness evaluation were destructive, samples were not repeatedly measured over time, and all observations were independent.

2.1.4. Data processing and model development

Quality change (ΔQ) for each sample was calculated as the relative change in quality with respect to its initial measured state. Specifically, ΔQ was computed as the difference between the quality parameter measured at a given time point and the corresponding initial quality measured prior to storage for the same sample.

All quality change observations were treated as independent data points, irrespective of the initial quality values or measurements obtained from other samples. Shelf-life partially depends on the initial quality (Mangaraj & Goswami, 2009). Each observation therefore represented a unique time–temperature condition and was used independently during model development.

Shelf-life for each sample was defined as the final storage day for which experimental measurements were available. In some cases, replicate samples became unavailable for color imaging and firmness evaluation due to visible surface mold development and spoilage during storage. Accordingly, the target quality change associated with shelf-life was calculated as the relative quality change obtained by subtracting the initial quality from the quality measured on the final day of storage for that sample. This final relative quality change was used as the target endpoint for shelf-life model development.

Data processing and model development were performed using Python (Google Colab, Python 3.13.2). Exploratory data analysis was conducted using Matplotlib (v3.10.3) and Seaborn (v0.12.0). Pearson correlation coefficients were calculated to evaluate relationships among quality parameters, gas composition, storage time, and temperature with significance testing (p-value < 0.05).

The dataset was divided into training (80%) and testing (20%) subsets and stratified five-fold cross-validation was applied with a separate validation dataset. Multiple regression-based and neural network-based modeling approaches were evaluated, including linear regression, decision tree regression, support vector regression, shallow neural networks, deep neural networks (Deep-NN), one-dimensional convolutional neural networks (1D-CNN), and deep neural decision trees (DNDT). Model development and architectures are described in the supplementary information.

Measured time, temperature, gas composition, and quality parameters were used as model inputs. Model configurations yielding the highest predictive performance, evaluated using the coefficient of determination (R^2), were retained. The input–output structure corresponding to the best-performing kinetic models developed in this section is illustrated in Fig. 2.

2.2. Remaining shelf-life (RSL) estimation and model validation

2.2.1. Experimental design for RSL estimation and simulated temperature abuse

Packaged cherries were subjected to simulated temperature abuse conditions to evaluate RSL prediction under variable storage environments. Prior to packaging in individual MAP bags, cherries were measured for weight, initial color, and firmness to establish baseline quality. Moderate temperature abuse consisted of exposure to 23 °C for 2 h, while extreme abuse involved exposure to 23 °C for 4 h, with five replicates per simulation. Temperature–time profiles were recorded using iButton® DS1921G-F50 data loggers (Analog Devices, Wilmington, MA, USA) placed both inside the packaging and in the surrounding environment. After 21 days of storage for each abuse scenario, final firmness and color measurements were collected and used to define threshold quality values for RSL estimation.

2.2.2. Respiration measurement

Respiration rates of sweet cherries were determined using a closed-jar system in which approximately 100 g of fruit were placed in sealed glass jars fitted with rubber septa to enable headspace gas sampling. Gas concentrations were measured periodically using a Dansensor® Checkpoint 3 (MOCON Inc., Minneapolis, MN, USA). Respiration experiments were conducted at 0, 4, 8, and 13 °C, and respiration rates for carbon dioxide production and oxygen consumption were estimated using least squares analysis in R (version 4.2). Temperature dependence of respiration was modeled using the Arrhenius equation as described by Mangaraj and Goswami (2011).

2.2.3. Physics-based gas composition estimation

Headspace gas composition under modified atmosphere packaging was estimated by coupling respiration kinetics with gas permeation through the packaging material. Temperature-dependent respiration

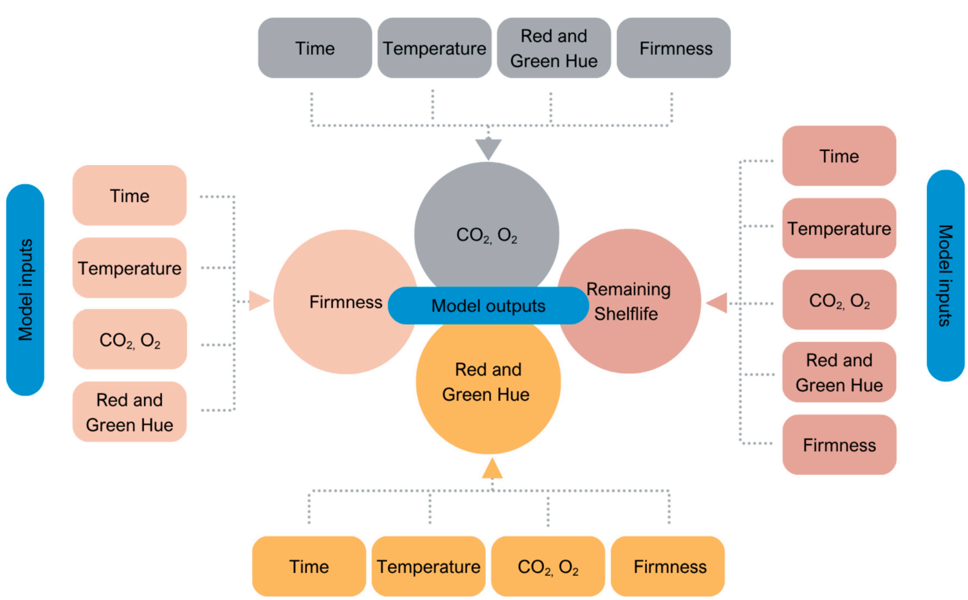

Fig. 2. Schematic representation of the input–output configuration used for kinetic model development of quality, gas composition, and shelf-life using measured data. The structure corresponds to the model configuration that yielded the highest predictive performance based on correlation analysis and coefficient of determination (R^2).

rates for carbon dioxide production and oxygen consumption were described using Arrhenius relationships, as expressed in Eqs. 1 and 2, with parameters obtained from respiration measurements.

$$R_{CO_2}^{t,T} = R_{CO_2}^{t-1,T_{ref}} \times \exp\left[\frac{-Ea_{CO_2}}{U}\left(\frac{1}{T}-\frac{1}{T_{ref}}\right)\right] \tag{1}$$

$$R_{O_2}^{t,T} = R_{O_2}^{t-1,T_{ref}} \times \exp\left[\frac{-Ea_{O_2}}{U}\left(\frac{1}{T}-\frac{1}{T_{ref}}\right)\right] \tag{2}$$

.

The amounts of carbon dioxide generated and oxygen consumed by the fruit over each time interval were calculated using mass balance expressions (Eqs. 3 and 4).

$$V_{CO_2}^{r,t} = w \times R_{CO_2}^{t,T} \times (t-(t-1)) \tag{3}$$

$$V_{O_2}^{r,t} = w \times R_{O_2}^{t,T} \times (t-(t-1)) \tag{4}$$

.

Gas permeation through the low-density polyethylene packaging film was computed using measured permeability values according to Eqs. 5 and 6 during the time interval $t-(t-1)$. The partial pressures $P_{CO_2}^{o}$ and $P_{O_2}^{o}$ are assumed to be 0 atm and 0.2093 atm to simplify.

$$V_{CO_2}^{p,t} = p_{CO_2} \times A \times \left(P_{CO_2}^{i,t-1} - P_{CO_2}^{o}\right) \tag{5}$$

$$V_{O_2}^{p,t} = p_{O_2} \times A \times \left(P_{O_2}^{o} - P_{O_2}^{i,t-1}\right) \tag{6}$$

.

Net gas accumulation within the package at a given time t and cumulative changes until time t were calculated using Eqs. 7–10.

$$V_{CO_2}^{t} = V_{CO_2}^{r,t} - V_{CO_2}^{p,t} \tag{7}$$

$$V_{O_2}^{t} = V_{O_2}^{p,t} - V_{O_2}^{r,t} \tag{8}$$

$$V_{CO_2}^{i,t} = V_{CO_2}^{t} + V_{CO_2}^{i,t-1} \tag{9}$$

$$V_{O_2}^{i,t} = V_{O_2}^{i,t-1} - V_{O_2}^{t} \tag{10}$$

.

Gas volumes were converted to partial pressures using the ideal gas law, as described by Eqs. 11 and 12.

$$P_{CO_2}^{t} = \frac{V_{CO_2}^{i,t}}{L} \tag{11}$$

$$P_{O_2}^{t} = \frac{V_{O_2}^{i,t}}{L} \tag{12}$$

.

2.2.4. RSL estimation

RSL was defined as the time required for a product to reach a predefined threshold quality level under dynamic storage conditions. Threshold quality (Q_{thr}) was defined operationally as the quality measured on the final sampling day under each corresponding storage condition. The threshold quality serving as the endpoint for RSL estimation was expressed as the relative quality change between the initial quality and the quality measured on the final sampling day for the same sample.

RSL was calculated using the shelf-life kinetic model expressed in Eq. 13, which integrates the deterioration rate over time and estimates the remaining duration before the threshold quality is reached. Inputs required for Eq. 13 included time–temperature history, partial pressures of oxygen and carbon dioxide, and instantaneous quality state (ΔQ) variables. Time and temperature were obtained from iButton® sensors, partial pressures of oxygen and carbon dioxide were obtained from physics-based gas composition estimation, and quality state variables were generated using a generative adversarial network (GAN), the architecture of which is provided in Figure S1 of the supplementary information.

$$RSL = NN\left(Q^{t}, \quad P_{CO_2}^{t}, P_{O_2}^{t}, t, \quad T\right) \tag{13}$$

.

The RSL model required quality state variables, including firmness factor, red hue angle, and green hue angle, which cannot be measured directly during real-time RSL estimation. Because these quality attributes are interdependent, estimating them using independent kinetic models is not feasible; therefore, a GAN was adopted to estimate their combined state. The GAN consisted of a generator and a discriminator trained using the same experimental dataset employed for the kinetic modeling, ensuring consistency across the framework. During training, the generator produced candidate quality states, and the discriminator evaluated their agreement with observed data. Detailed architecture is provided in the supplementary information. After training, the Generator was used to estimate internally consistent quality state variables, which were then used as inputs to Eq. 13 during RSL estimation. The complete workflow for real-time RSL estimation, integrating sensor-based time–temperature data, physics-based gas composition estimation, GAN-based quality state generation, and shelf-life calculation, is illustrated in Fig. 3.

The supplementary information provides detailed methodological and modeling components supporting the RSL framework presented in the main manuscript. It includes implementation details, architectures, hyperparameter optimization strategies, and evaluation procedures for multiple machine-learning and deep-learning models used for quality attribute and gas composition estimation, including linear regression, decision tree regression, support vector regression, shallow neural networks, Deep-NN, 1D-CNN, DNDT, and GAN. Additional supplementary results include expanded analyses of gas composition dynamics, firmness and color prediction performance, and representative model outputs under controlled storage conditions. These supplementary materials were retained separately to provide detailed technical documentation while maintaining the primary focus of the main manuscript on the integrated RSL prediction framework under modified atmosphere packaging and variable cold-chain conditions.

3. Results and discussions

3.1. Effects of time and temperature on cherry quality and shelf-life prediction under controlled MAP storage

Controlled storage experiments were conducted to characterize quality evolution and shelf-life behavior of Bing sweet cherries under MAP and to establish the modeling foundation for subsequent RSL analysis. The results presented here emphasize dominant trends and interdependencies relevant to shelf-life modeling rather than detailed physiological interpretation of individual quality attributes.

3.1.1. Response of MAP gas composition and quality attributes under controlled storage

Across all storage temperatures, oxygen concentration decreased while carbon dioxide accumulated over time, as shown in Figure S2 of the supplementary information, reflecting temperature-dependent respiratory activity within the package. Elevated storage temperatures (8 °C and 13 °C) resulted in rapid oxygen depletion and accelerated carbon dioxide accumulation, whereas storage at 0 °C and 4 °C maintained near-aerobic conditions for substantially longer periods. A pronounced non-linear transition was observed between 4 °C and 8 °C, where

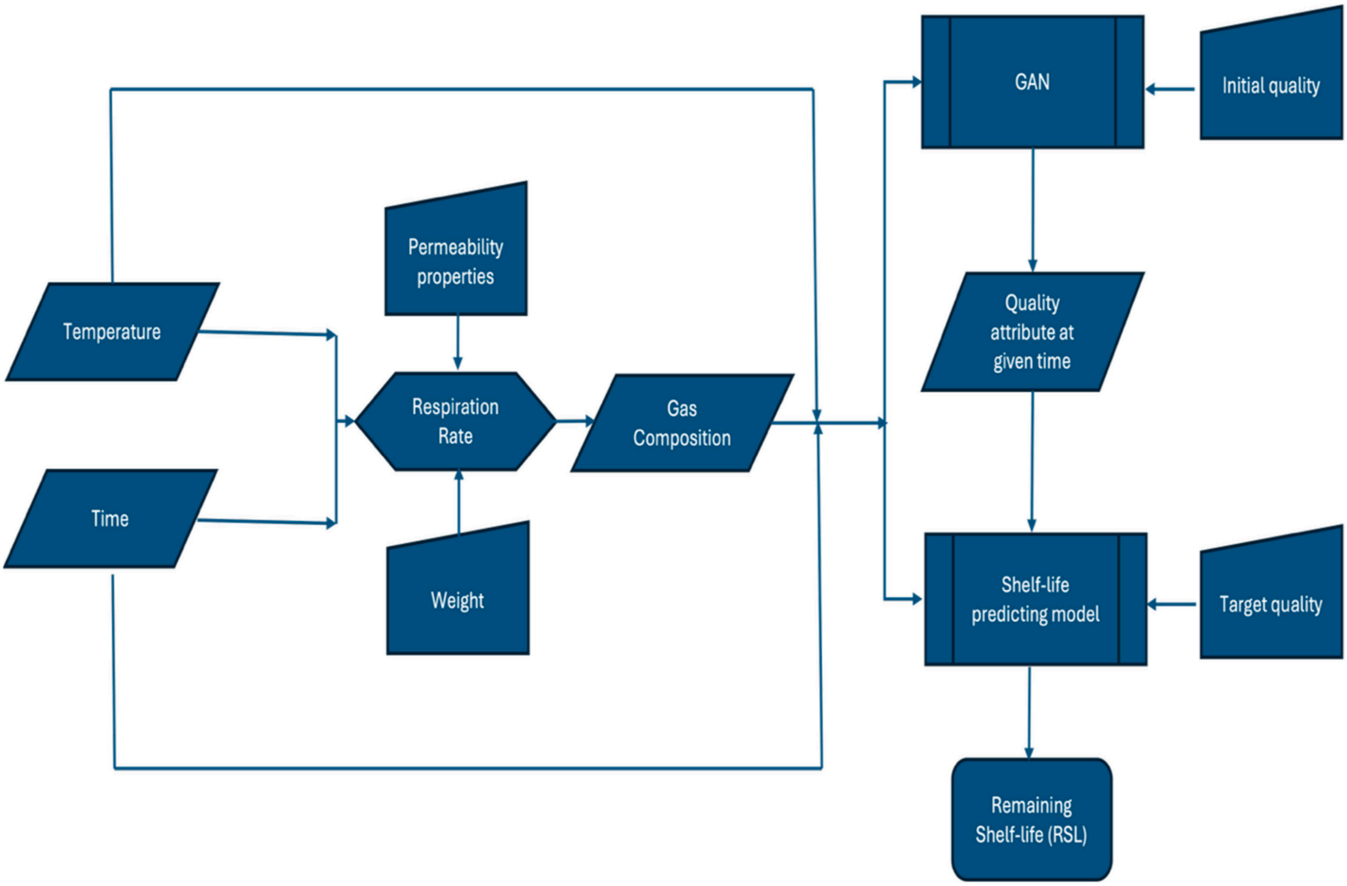

Fig. 3. Schematic of the remaining shelf-life prediction framework integrating respiration-based kinetics, MAP gas exchange, and data-driven estimation of quality state variables. Temperature history drives respiration and gas composition modeling, while a generative adversarial network, trained on the same experimental dataset, provides internally consistent quality states. All model inputs are combined according to Eq. 13 to estimate RSL under dynamic cold-chain conditions.

relatively small temperature increases produced disproportionate changes in gas composition dynamics.

Temperature-dependent trends in firmness and color attributes followed a similar pattern. Cherries stored at higher temperatures exhibited faster firmness loss and accelerated pigment degradation, while lower storage temperatures delayed quality deterioration. Firmness declined most rapidly at 8 °C and 13 °C, whereas storage at 0 °C and 4 °C preserved textural integrity for extended durations. Changes in color attributes further reflected thermal sensitivity, with a green hue associated with stem chlorophyll (Xin et al., 2021), responding more rapidly to temperature stress than red hue, associated with fruit surface color. However, the present framework extends these observations by integrating multiple quality attributes within a dynamic remaining shelf-life prediction approach under MAP conditions. Additional details regarding the effects of storage time and temperature on the measured quality attributes are provided in the supplementary information. Specifically, Figure S3 presents the changes in firmness, while Figures S4 and S5 illustrate the corresponding changes in hue angle and saturation, respectively.

Although gas composition, firmness, and color attributes responded consistently to temperature, their temporal trajectories differed, indicating asynchronous degradation processes. These differences highlight that deterioration under MAP is governed by coupled but non-uniform physiological responses, limiting the usefulness of single-attribute indicators for shelf-life assessment. From a modeling perspective, gas composition serves as an integrative indicator of respiration-driven response to temperature history, while quality attributes provide complementary but partially decoupled signals of deterioration. Extended gas composition profiles and detailed analyses of firmness and color evolution are provided in the supplementary information.

3.1.2. Interdependency among quality parameters

Relationships among temperature, gas composition, firmness, and color attributes are summarized in the correlation matrix shown in Fig. 4. Strong associations were observed between temperature and gas composition variables, whereas firmness degradation showed a stronger dependence on storage duration. Color attributes exhibited weaker and less consistent correlations with atmospheric variables, suggesting partially independent degradation pathways.

These results indicate that no single quality parameter adequately represents overall deterioration under MAP, particularly when storage conditions vary. From a shelf-life modeling standpoint, the partial decoupling among quality attributes reinforces the need for integrated, multivariate prediction frameworks rather than rule-based or threshold-driven approaches. Extended correlation analysis is included in the supplementary information.

3.1.3. Estimation of quality attributes and shelf-life

Model performance for estimating gas composition, firmness, color attributes, and shelf-life under controlled storage conditions is summarized in Table 1. Comparative performance of deep learning models for gas composition estimation, firmness, and color estimation is shown in Figures S5–S8 of the supplementary information, respectively. Across the predicted variables evaluated in this study, deep-learning architectures consistently outperformed traditional regression and shallow-learning models. Similar advantages of deep-learning approaches have been reported for shelf-life and quality prediction in apples (Cao et al., 2021), mushrooms (Fu et al., 2019), and strawberries (Qiao et al.,

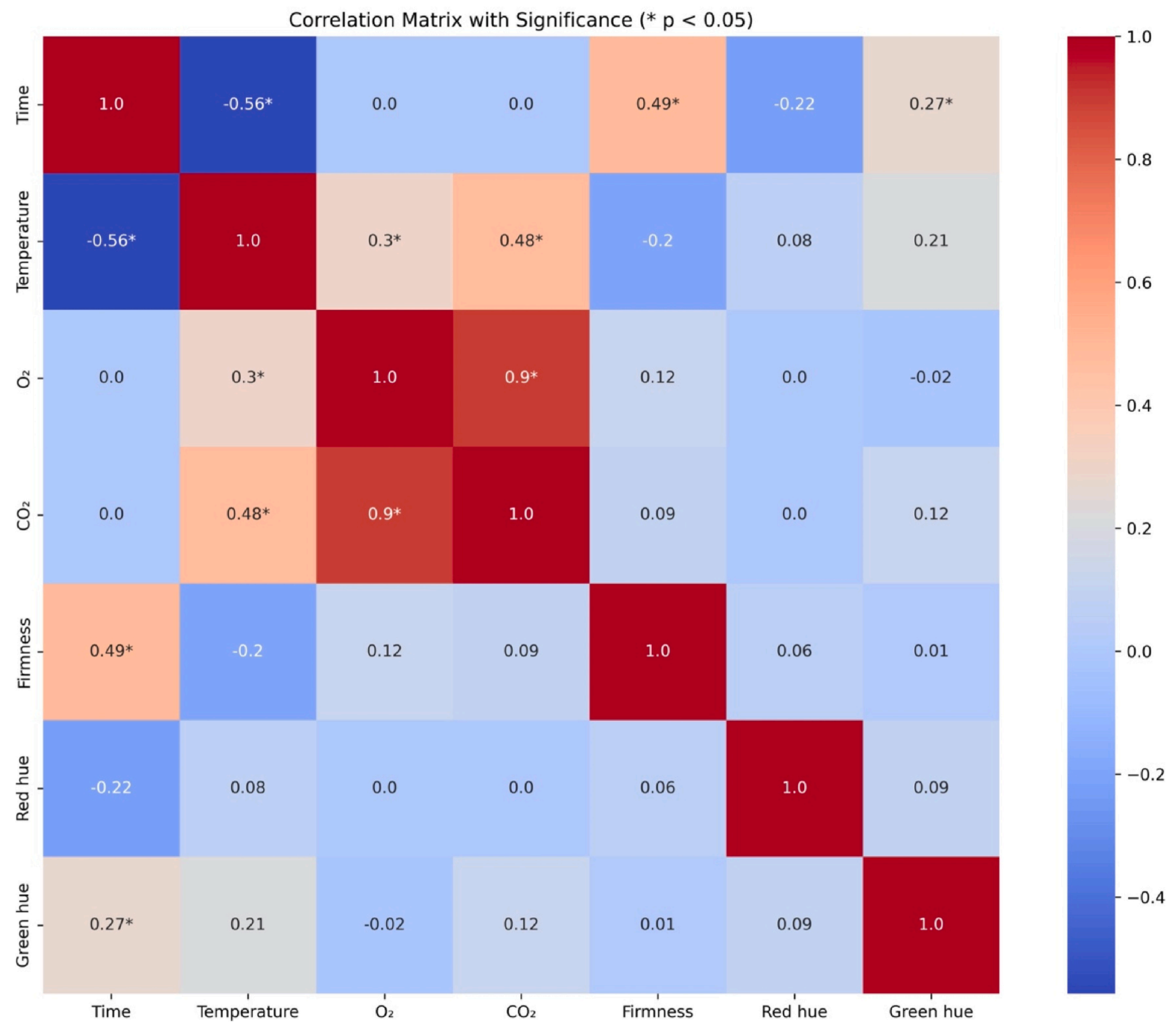

Fig. 4. Correlation matrix showing relationships among storage temperature, MAP gas composition (O_2 and CO_2), firmness, and color attributes of sweet cherries under controlled storage conditions. The matrix highlights differences in coupling strength among physiological and quality variables relevant to shelf-life modeling. '*' represents that correlation is significant (p-value < 0.05).

Table 1
Model performance matrix for estimating cherry quality and shelf-life.

Models	Partial pressure of CO_2 (atm)		Partial pressure of O_2 (atm)		Mean Firmness (g mm^{-1})		Maximum Hue angle at Red (°)		Maximum Hue angle at Green (°)		Shelf-life (days)	
	R^2	RMSE	R^2	RMSE	R^2	RMSE	R^2	RMSE	R^2	RMSE	R^2	RMSE
Linear Regression	0.171	0.936	−0.165	1.66	−0.0168	33.7	−0.158	2.40	−0.0628	4.38	0.598	6.20
Decision Tree Regression	−0.452	1.19	−0.393	1.75	−0.732	44.5	0.363	1.66	−0.823	5.57	0.678	5.49
SVR	−0.0603	1.07	−0.109	1.63	0.337	27.2	−0.0527	2.29	0.0532	4.22	0.0721	10.0
SNN	−5.66	1.83	−2.54	2.57	−0.0365	31.2	−5.28	3.88	−0.296	4.20	−4.95	15.0
Deep-NN	0.846	0.442	0.689	1.00	0.919	10.5	0.806	0.976	0.803	0.982	0.833	4.32
1D-CNN	0.823	0.473	0.661	1.043	0.635	22.2	0.616	1.37	0.775	2.14	0.991	1.01
DNDT	−2.08	1.94	−1.65	3.04	−0.801	59.4	−0.324	5.74	−0.393	5.83	−0.668	12.3

2022), where complex, nonlinear relationships among storage conditions and quality attributes influence product deterioration over time. Higher standard deviation and lower prediction accuracy of Deep-NN compared to 1D-CNN in shelf life estimation seems to arise due to inability of artificial neural network (ANN) models to consider the time dependent information for prediction. The shelf life of the cherries has been found to be more dependent on past quality parameters of cherries. However, Deep-NN provide comparable predictions for quality attributes which provides the impression that the quality metrics are less dependent on previous quality parameters (less sequential or time dependent) compared to shelf-life estimation.

Despite high predictive accuracy for individual quality attributes, their interdependency and asynchronous degradation limited their direct applicability for shelf-life inference. Acceptable values of one attribute frequently coincided with advanced deterioration in another, and sequential prediction frameworks introduced compounded uncertainty. Expanded model performance comparisons are provided in the supplementary information.

3.1.4. Shelf-life prediction under controlled storage

Direct shelf-life prediction results (predicted vs actual values) under controlled storage conditions for Deep-NN and 1D-CNN are shown in Fig. 5, and other models and their corresponding performance metrics summarized in Table 1. Among all evaluated approaches, deep learning models achieved superior predictive accuracy, with the one-dimensional convolutional neural network providing the lowest prediction error and strongest agreement with observed shelf-life. This performance reflects the model's ability to learn combined deterioration patterns driven by time, temperature history, gas dynamics, and quality evolution.

Shelf-life prediction in this section represents estimation of total storage duration until a predefined quality threshold is reached under known and complete storage histories. In contrast, RSL prediction requires continuous estimation of the time remaining to reach that threshold at intermediate points, accounting for cumulative and potentially irreversible effects of prior handling and temperature exposure. The shelf-life models developed here therefore establish baseline deterioration behavior and provide the foundation for extending prediction to RSL under dynamic cold-chain conditions, which is addressed in the following section.

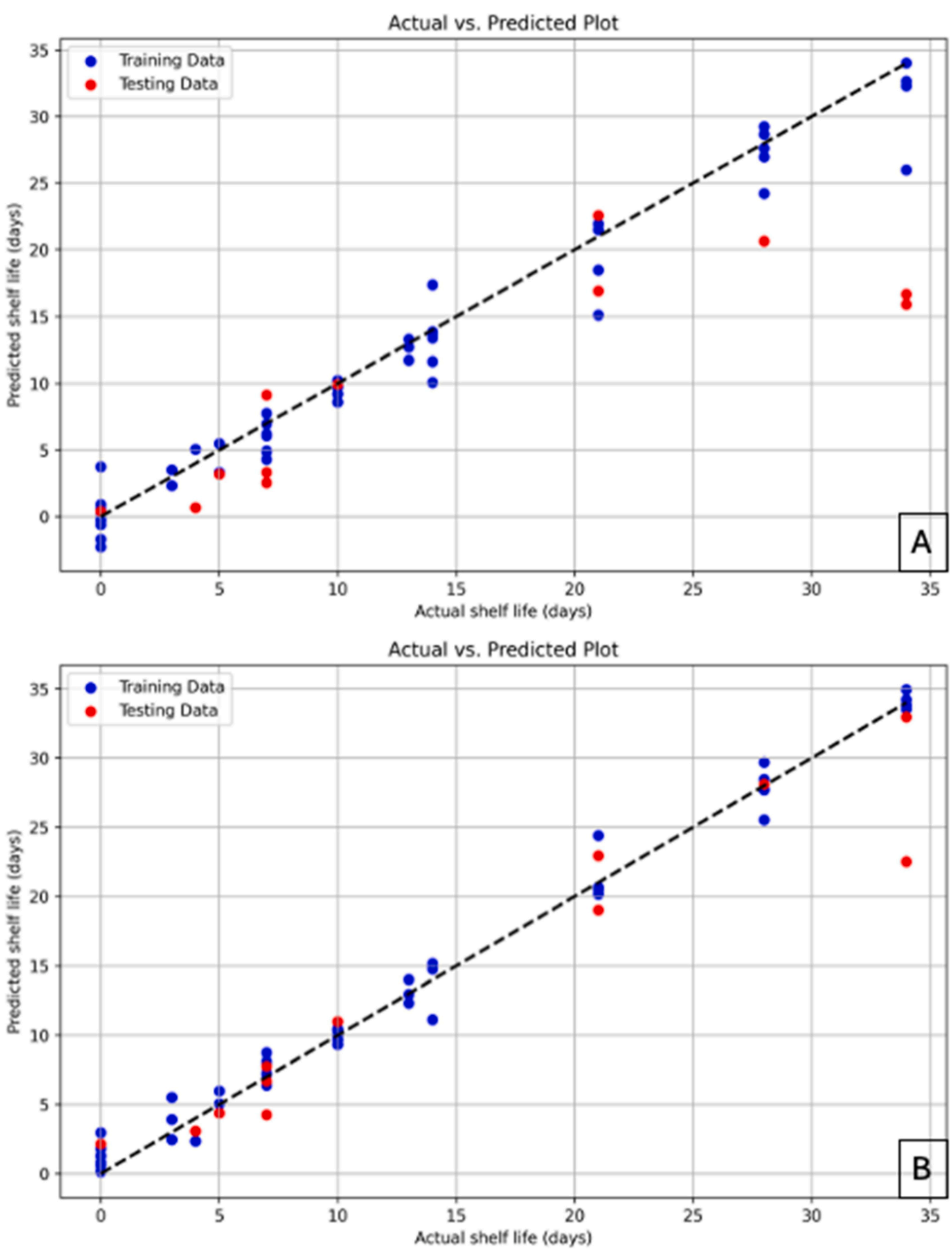

Fig. 5. Comparison of predicted and observed shelf-life for sweet cherries under controlled storage conditions using (A) a deep neural network and (B) a one-dimensional convolutional neural network. The figure illustrates differences in model performance for capturing shelf-life behavior based on time, temperature history, gas composition, and quality attributes.

3.2. Remaining shelf-life prediction under simulated cold-chain abuse conditions

The behavior of RSL was evaluated under simulated cold-chain conditions involving transient temperature fluctuations. The analysis integrates respiration-driven MAP responses with model-based predictions to assess how non-uniform thermal histories influence remaining shelf-life under moderate and extreme abuse scenarios.

3.2.1. Temperature dependence of respiration

The temperature dependence of respiration rates for carbon dioxide production and oxygen consumption followed Arrhenius behavior, as shown in Fig. 6. Activation energies estimated for CO_2 and O_2 respiration were 104.54 kJ mol^{-1} and 106.91 kJ mol^{-1} , respectively, which fall within the expected biological range for enzymatic processes in fresh produce (Mundim et al., 2020). Carbon dioxide production exhibited slightly greater sensitivity to temperature changes than oxygen consumption, indicating that proportional increases in CO_2 are expected to dominate respiratory response under fluctuating thermal conditions.

This differential sensitivity has direct implications for MAP performance during temperature abuse events, where short-duration increases in temperature can rapidly alter internal gas composition even when average storage temperatures remain within acceptable limits.

3.2.2. Time-temperature abuse profiles

Representative time–temperature profiles and gas composition evolution imposed during storage are illustrated in Figs. 7 and 8 for moderate and extreme abuse scenarios respectively. Each profile consisted of seven discrete temperature peaks designed to simulate repeated cold-chain disruptions. In the moderate scenario, samples were exposed to 23 °C for 2 h per event, whereas the extreme scenario extended exposure to 4 h. Peak temperatures reached approximately 17 °C and 22 °C for the moderate and extreme scenarios, respectively, relative to a refrigerated baseline near 6 °C. Details are provided in supplementary information Figure S9. The higher magnitude and longer duration of temperature peaks in the extreme scenario resulted in a substantially greater thermal load. Although brief, these excursions produced gas composition profiles different from previously designed conditions, accelerating deterioration disproportionately relative to mean temperature alone (Mangaraj & Goswami, 2011).

3.2.3. MAP gas composition response during temperature abuse

During each temperature excursion, carbon dioxide partial pressure increased sharply while oxygen partial pressure decreased, reflecting the immediate respiratory response to elevated temperature. Under moderate abuse, oxygen partial pressure decreased to approximately 0.15 atm while carbon dioxide increased to about 0.12 atm during peak exposure. More pronounced deviations were observed under extreme abuse, where oxygen dropped to approximately 0.13 atm and carbon dioxide increased to approximately 0.14 atm. These deviations occurred consistently during the highest temperature peaks, confirming that transient thermal conditions, rather than cumulative storage time alone, governed gas composition dynamics.

Following abuse events, gas concentrations did not fully return to their original trajectories, a behavior previously reported in MAP-stored strawberries (Xanthopoulos et al., 2012) and pears (Xanthopoulos et al., 2017) exposed to transient temperature fluctuations. The slower recovery of oxygen relative to carbon dioxide is consistent with the greater permeability of LDPE films to CO_2 than O_2 reported in these studies. This asymmetry highlights the interaction between respiration kinetics and packaging properties and demonstrates how short-term temperature stress can induce lingering atmospheric effects within MAP systems.

The transient CO_2 concentrations achieved during abuse overlapped with ranges previously reported to influence cherry quality, including firmness retention and decay suppression (Wang & Long, 2014; Xing et al., 2025). Similar responses have been reported in sweet cherries stored under MAP, where temperature fluctuations substantially increased respiration demand and disrupted equilibrium gas compositions, resulting in transient atmospheric conditions that differed from those predicted under steady storage temperatures (Petracek et al., 2002). However, the repeated and short-duration nature of the excursions observed in the present study suggests that such conditions differ fundamentally from the steady-state atmospheres typically assumed during MAP design.

Similar deviations from equilibrium atmospheres following temperature fluctuations have also been reported in other MAP systems, where thermal heterogeneity, transient gas responses, and non-equilibrium package behavior persisted beyond the duration of the temperature

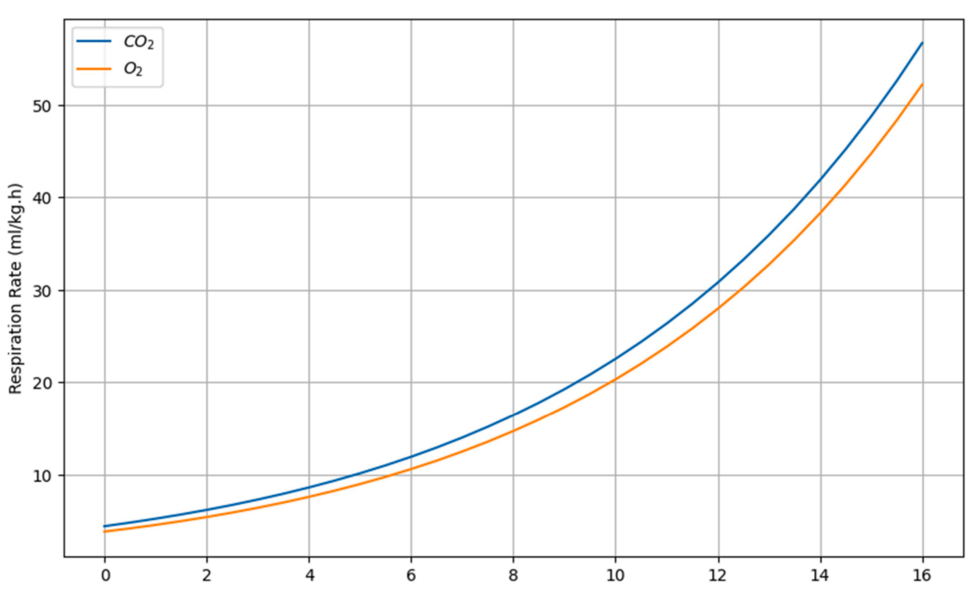

Fig. 6. Temperature dependence of respiration rates for oxygen consumption and carbon dioxide production in sweet cherries, modeled using the Arrhenius relationship. The fitted curves illustrate differences in temperature sensitivity between O_2 and CO_2 respiration relevant to remaining shelf-life prediction under variable cold-chain conditions.

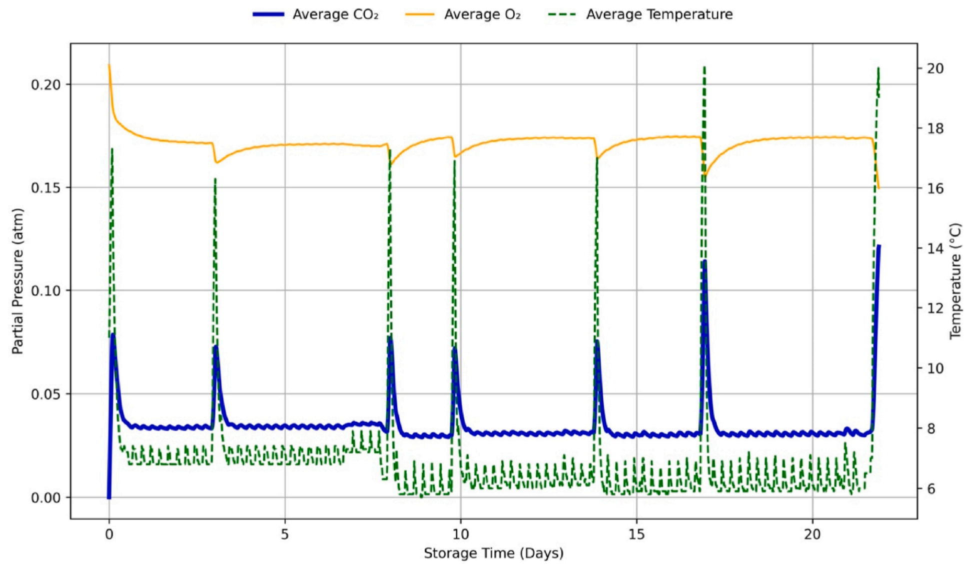

Fig. 7. Predicted internal oxygen and carbon dioxide partial pressures under modified atmosphere packaging during moderate temperature abuse. Transient deviations in gas composition reflect respiration-driven responses to short-term temperature excursions.

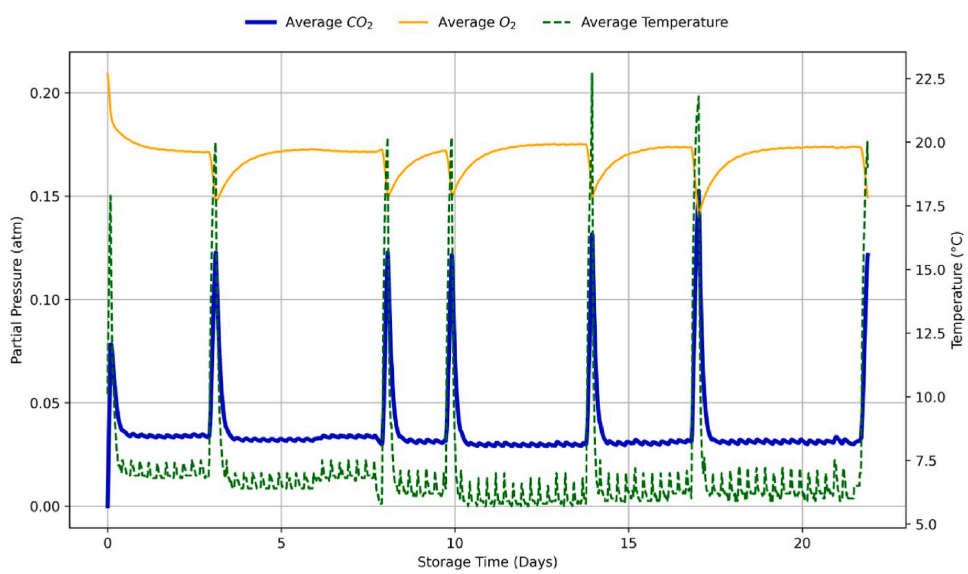

Fig. 8. Predicted internal oxygen and carbon dioxide partial pressures under modified atmosphere packaging during extreme temperature abuse. Larger and more prolonged temperature excursions result in greater deviations in gas composition compared to moderate abuse conditions.

disturbance (Defraeye et al., 2024; Zhang et al., 2026). Although MAP provides a buffering effect that facilitates partial recovery toward the designed gas composition following temperature excursions, these transient shifts reflect cumulative stress rather than controlled atmosphere optimization.

As a result, conventional shelf-life estimates based on steady storage conditions may be insufficient under variable cold-chain environments. Short-term temperature abuse can induce dynamic gas responses within MAP systems that continue to influence product deterioration and remaining shelf-life beyond the transient event itself.

Traditional kinetic approaches based on ordinary differential equations and Arrhenius-type temperature dependence have been widely used to model postharvest deterioration under dynamic storage conditions. Multiple mechanistic approaches may be appropriate depending on the produce commodity, cultivar, physiological response, and storage system being studied. While such approaches effectively describe individual physiological processes, the present framework emphasizes integration of multiple interacting quality attributes and transient MAP responses within a unified data-driven remaining shelf-life prediction system under variable cold-chain conditions.

3.2.4. RSL prediction under temperature abuse

The impact of fluctuating temperature conditions on RSL was evaluated using the shelf-life prediction models developed under controlled storage conditions. Among the evaluated approaches, the 1D-CNN consistently achieved the lowest prediction error and highest accuracy; therefore, all RSL results presented in this section are based on the 1D-CNN model.

Predicted RSL trajectories for the moderate and extreme abuse scenarios are presented in Fig. 9. Under ideal storage conditions without abuse, remaining shelf-life declined gradually over time. In contrast, both abuse scenarios exhibited abrupt reductions in predicted RSL during temperature peaks. Each abuse event resulted in a discrete loss of remaining shelf-life, followed by partial recovery upon return to

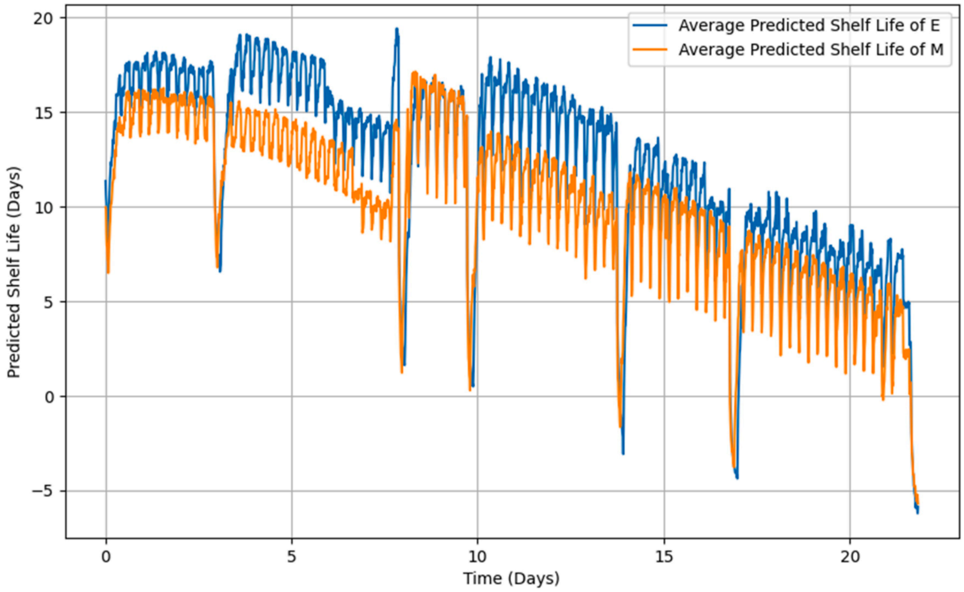

Fig. 9. Predicted remaining shelf-life (RSL) trajectories of sweet cherries under moderate (M) and extreme (E) temperature abuse scenarios. Stepwise reductions in RSL correspond to temperature excursions, illustrating cumulative shelf-life loss under variable cold-chain conditions compared to uninterrupted refrigerated storage.

refrigerated conditions.

On average, individual abuse events resulted in the loss of approximately one to two additional days of remaining shelf-life. Repeated exposure produced cumulative effects, leading to progressively lower RSL trajectories, particularly under extreme abuse conditions. These results indicate that transient temperature abuse contributes to partially irreversible reductions in future storage potential, even when optimal temperatures are subsequently restored.

Model performance across individual replicates is summarized in Table 2, which reports RMSE values for the Deep-NN, 1D-CNN, and DNDT models under both moderate and extreme abuse scenarios. The 1D-CNN consistently outperformed the other models across all replicates, demonstrating greater robustness under dynamic temperature conditions.

Prediction uncertainty over storage time is illustrated in Fig. 10, which shows the absolute prediction error of the 1D-CNN model. Errors were highest during the early stages of storage, particularly under extreme abuse, with peak deviations observed around Day 14. As storage progressed, prediction error decreased, indicating improved stability as physiological changes became more gradual.

3.2.5. Application of RSL prediction and future scope

The RSL trajectories obtained under simulated cold-chain abuse conditions demonstrate how transient temperature deviations translate into quantifiable and cumulative losses in remaining product life. Stepwise reductions in RSL during abuse events indicate that temperature variability affects not only immediate deterioration rates but also subsequent deterioration trajectories.

Although partial recovery in predicted RSL was observed following a return to refrigerated conditions, recovery occurred along a shifted trajectory, suggesting that a portion of the shelf-life loss was irreversible. This behavior reflects cumulative physiological damage induced during thermal stress and cannot be captured using static shelf-life estimates derived from constant-temperature storage.

From an application perspective, RSL prediction provides a single, time-resolved indicator that integrates the combined effects of temperature history, respiration behavior, MAP gas dynamics, and quality evolution. This integration reduces reliance on individual quality attributes that may degrade asynchronously and exhibit weak interdependence. As demonstrated here, acceptable levels of firmness or color can coexist with substantially reduced remaining life, limiting the usefulness of attribute-specific thresholds for operational decision-making.

The framework developed in this study is well suited for extension toward real-world cold-chain applications. Integration of real-time sensing technologies would allow continuous updating of RSL predictions throughout storage and transport. Further refinement through incorporation of probabilistic indicators for stochastic spoilage events, commercially relevant defects such as mold development and pitting, and larger datasets generated across seasons, growing locations, cultivars, and commercial handling systems could enhance robustness under commercial conditions. Future improvements in imaging methodologies and cultivar-specific quality indicators may also help reduce variability associated with color-related measurements. Although parameterized for Bing sweet cherries, the structure of the framework is not commodity-specific and can be adapted to other fresh produce by substituting appropriate physiological parameters, quality indicators, and acceptability thresholds.

4. Conclusion

This study presents an integrated framework for modeling postharvest deterioration of sweet cherries under MAP by combining respiration behavior, gas exchange, quality evolution, and data-driven prediction. The results indicate that deterioration under realistic cold-

Table 2
Performance summary of Deep-NN, 1D-CNN, and DNDT for predicting remaining shelf-life for individual samples in terms of RMSE (Days).

	Extreme temperature abuse					Moderate temperature abuse				
Model/Replicate	**1**	**2**	**3**	**4**	**5**	**1**	**2**	**3**	**4**	**5**
Deep-NN	33.2	8.7	8.5	10.0	7.9	9.1	7.6	9.2	10.2	6.1
1D-CNN	4.6	4.8	4.2	4.1	8.1	3.9	3.6	4.6	4.0	4.9
DNDT	11.7	11.6	11.7	11.6	11.6	11.7	11.7	11.6	11.6	11.7

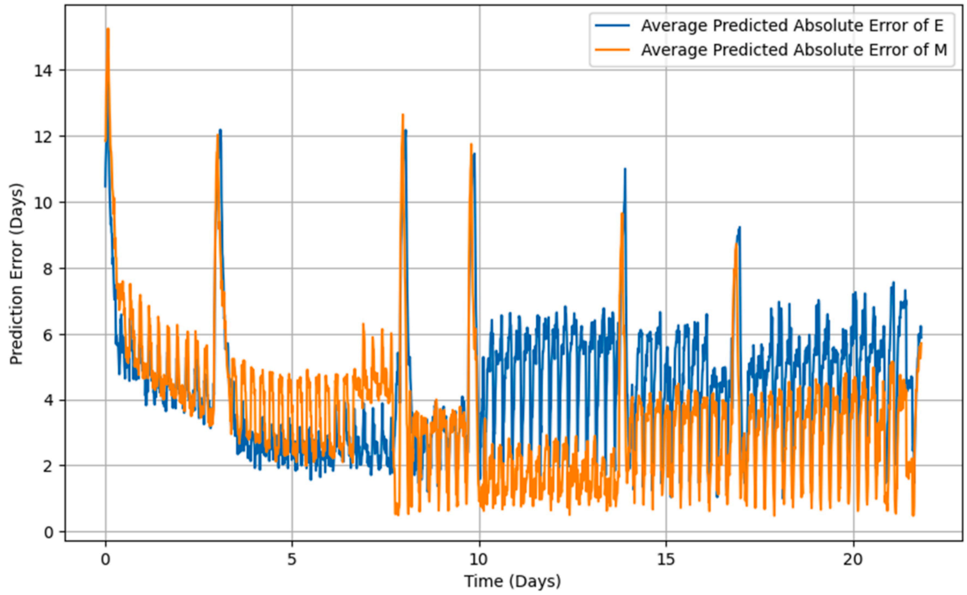

Fig. 10. Absolute prediction error of the remaining shelf-life (RSL) model over storage time under moderate (M) and extreme (E) temperature abuse scenarios. Higher errors during early storage reflect increased sensitivity to transient thermal stress, with improved stability as storage progresses.

chain conditions is governed by cumulative interactions among temperature history and physiological response, rather than by static storage assumptions or isolated quality metrics. Accordingly, predictive approaches that integrate multiple signals provide a more realistic representation of postharvest behavior than constant-temperature shelf-life estimates.

The framework further demonstrates that remaining shelf-life prediction benefits from treating quality degradation as a systems-level process, where asynchronous changes in gas composition, texture, and visual attributes collectively determine usability. By learning these interactions directly from data, the modeling approach links physiological response to time-resolved usability without reliance on fixed thresholds, supporting interpretation of deterioration under variable conditions.

Because the models are inherently data-driven, their robustness and reproducibility depend on the breadth of conditions represented in the training data. For Bing sweet cherries, continued expansion of training data across locations, seasons, and handling practices will enhance the robustness and reproducibility of the proposed framework. Additionally, the framework can be further expanded by incorporating commercially relevant quality defects such as mold development, pitting, stem browning, and other cultivar- or storage-specific disorders to improve applicability under broader commercial conditions. In this context, the contribution of this manuscript lies in consolidating physiological understanding and data-driven modeling into a unified framework, rather than presenting a finalized commercial tool.

Overall, this work establishes a methodological foundation for remaining shelf-life modeling that can be progressively strengthened through broader data integration, supporting more informed decision-making and reduced losses in perishable supply chains.

CRediT authorship contribution statement

Smit Patel: Writing – review & editing, Writing – original draft, Visualization, Validation, Investigation, Formal analysis, Data curation, Conceptualization. **Juming Tang:** Writing – review & editing. **Kang Huang:** Writing – review & editing, Supervision, Funding acquisition, Conceptualization. **Rishabh Goyal:** Writing – review & editing, Writing – original draft, Visualization, Validation, Investigation, Formal analysis. **Torres Carolina A:** Writing – review & editing, Writing – original draft, Visualization, Methodology, Data curation, Conceptualization. **Charles L Munson:** Writing – review & editing. **Sablani Shyam:** Writing – review & editing, Visualization, Supervision, Funding acquisition, Conceptualization.

Declaration of Competing Interest

The authors declare that they have no known competing financial interests or personal relationships that could have appeared to influence the work reported in this paper.

Acknowledgement

This research was partially supported by the USDA National Institute of Food and Agriculture Hatch project #1016366. We gratefully acknowledge Allan Brothers, Inc. for providing the Bing cherries and packaging materials used in this study. We also thank Dr. Ashish Kondal for his invaluable assistance with image-processing tasks.

Appendix A. Supporting information

Supplementary data associated with this article can be found in the online version at doi:10.1016/j.fpsl.2026.101808.

Data availability

Data will be made available on request.

References

Cao, M., Wang, D., Qiu, L., Ren, X., & Ma, H. (2021). Shelf life prediction of 'Royal Gala' apples based on quality attributes and storage temperature. *Korean Journal of Horticultural Science and Technology, 39*, 343–355. https://doi.org/10.7235/HORT.20210031

Chaix, E., Broyart, B., Couvert, O., Guillaume, C., Gontard, N., & Guillard, V. (2015). Mechanistic model coupling gas exchange dynamics and Listeria monocytogenes growth in modified atmosphere packaging of non respiring food. *Food Microbiology, 51*, 192–205. https://doi.org/10.1016/j.fm.2015.05.017

Chen, Q., Li, J., Yang, H., & Qian, J. (2023). A dynamic shelf-life prediction method considering actual uncertainty: Application to fresh fruits in long-term cold storage. *Journal of Food Engineering, 349*, Article 111471. https://doi.org/10.1016/j.jfoodeng.2023.111471

Cui, F., Zheng, S., Wang, D., Tan, X., Li, Q., Li, J., & Li, T. (2023). Recent advances in shelf life prediction models for monitoring food quality. *Comprehensive Reviews in*

Food Science and Food Safety, 22, 1257–1284. https://doi.org/10.1111/1541-4337.13110
Defraeye, T., Verreydt, C., Gonthier, J., Lukasse, L., Cronje, P., & Berry, T. (2024). The virtual container: Physics-based simulation of refrigerated container map temperature and fruit quality evolution and variability in a shipment. *Postharvest Biology and Technology, 211*, Article 112722. https://doi.org/10.1016/j.postharvbio.2023.112722
Fu, Z., Zhao, S., Zhang, X., Polovka, M., & Wang, X. (2019). Quality characteristics analysis and remaining shelf life prediction of fresh tibetan tricholoma matsutake under modified atmosphere packaging in cold chain. *Foods, 8*, 136. https://doi.org/10.3390/foods8040136
Goyal, K., Kumar, P., & Verma, K. (2024). Tomato ripeness and shelf-life prediction system using machine learning. *Food Measure, 18*, 2715–2730. https://doi.org/10.1007/s11694-023-02349-x
Habib, M., Bhat, M., Dar, B. N., & Wani, A. A. (2017). Sweet cherries from farm to table: A review. *Critical Reviews in Food Science and Nutrition, 57*, 1638–1649. https://doi.org/10.1080/10408398.2015.1005831
Joshi, K., Tiwari, B., Cullen, P. J., & Frias, J. M. (2019). Predicting quality attributes of strawberry packed under modified atmosphere throughout the cold chain. *Food Packaging and Shelf Life, 21*, Article 100354. https://doi.org/10.1016/j.fpsl.2019.100354
Koutsimanis, G., Harte, J., & Almenar, E. (2015). Development and evaluation of a new packaging system for fresh produce: A case study on fresh cherries under global supply chain conditions. *Food and Bioprocess Technology, 8*, 655–669. https://doi.org/10.1007/s11947-014-1437-0
Le Nguyen, L. P., Visy, A., Baranyai, L., Friedrich, L., & Mahajan, P. V. (2020). Application of hue spectra fingerprinting during cold storage and shelf-life of packaged sweet cherry. *Food Measure, 14*, 2689–2702. https://doi.org/10.1007/s11694-020-00515-z
Mangaraj, S., & Goswami, T. K. (2009). Modified atmosphere packaging of fruits and vegetables for extending shelf-life-A review. *Fresh produce, 3*, 1–31.
Mangaraj, S., & Goswami, T. K. (2011). Measurement and Modeling of Respiration Rate of Guava (CV. Baruipur) for Modified Atmosphere Packaging. *International Journal of Food Properties, 14*, 609–628. https://doi.org/10.1080/10942910903312403
Mundim, K. C., Baraldi, S., Machado, H. G., & Vieira, F. M. C. (2020). Temperature coefficient (Q10) and its applications in biological systems: Beyond the Arrhenius theory. *Ecological Modelling, 431*, Article 109127. https://doi.org/10.1016/j.ecolmodel.2020.109127
Nguyen, L. L. P., Baranyai, L., Nagy, D., Mahajan, P. V., Zsom-Muha, V., & Zsom, T. (2021). Color analysis of horticultural produces using hue spectra fingerprinting. *MethodsX, 8*, Article 101594. https://doi.org/10.1016/j.mex.2021.101594
Petracek, P. D., Joles, D. W., Shirazi, A., & Cameron, A. C. (2002). Modified atmosphere packaging of sweet cherry (Prunus avium L., ev. 'Sams') fruit: Metabolic responses to oxygen, carbon dioxide, and temperature. *Postharvest Biology and Technology, 24*, 259–270. https://doi.org/10.1016/S0925-5214(01)00192-2
Porter, S. D., Reay, D. S., Higgins, P., & Bomberg, E. (2016). A half-century of production-phase greenhouse gas emissions from food loss & waste in the global food supply chain. *Science of The Total Environment, 571*, 721–729. https://doi.org/10.1016/j.scitotenv.2016.07.041
Qiao, J., Guo, M., Wu, Y., Gao, J., & Yue, Z. (2022). Research on strawberry cold chain transportation quality perception method based on BP neural network. *Applied Sciences, 12*, 8872. https://doi.org/10.3390/app12178872
Sandhya. (2010). Modified atmosphere packaging of fresh produce: Current status and future needs. *LWT - Food Science and Technology, 43*, 381–392. https://doi.org/10.1016/j.lwt.2009.05.018
Shi, C., Zhao, Zhiyao, Jia, Zhixin, Hou, Mengyuan, Yang, Xinting, Ying, Xiaoguo, & Ji, Z. (2024). Artificial neural network-based shelf life prediction approach in the food storage process: A review. *Critical Reviews in Food Science and Nutrition, 64*, 12009–12024. https://doi.org/10.1080/10408398.2023.2245899
Shukla, M., & Jharkharia, S. (2013). Agri-fresh produce supply chain management: A state-of-the-art literature review. *International Journal of Operations & Production Management, 33*, 114–158. https://doi.org/10.1108/01443571311295608
Torres-Sánchez, R., Martínez-Zafra, M. T., Castillejo, N., Guillamón-Frutos, A., & Artés-Hernández, F. (2020). Real-time monitoring system for shelf life estimation of fruit and vegetables. *Sensors, 20*, 1860. https://doi.org/10.3390/s20071860
Tsironi, T., Dermesonlouoglou, E., Giannoglou, M., Gogou, E., Katsaros, G., Taoukis, P., 2017. Shelf-life prediction models for ready-to-eat fresh cut salads: Testing in real cold chain. International Journal of Food Microbiology, Special Issue: 9th International Conference on Predictive Modelling in Food (Rio de Janeiro, Brazil) 240, 131–140. https://doi.org/10.1016/j.ijfoodmicro.2016.09.032.
Wang, Y., & Long, L. E. (2014). Respiration and quality responses of sweet cherry to different atmospheres during cold storage and shipping. *Postharvest Biology and Technology, 92*, 62–69. https://doi.org/10.1016/j.postharvbio.2014.01.003
Xanthopoulos, G., Koronaki, E. D., & Boudouvis, A. G. (2012). Mass transport analysis in perforation-mediated modified atmosphere packaging of strawberries. *Journal of Food Engineering, 111*, 326–335. https://doi.org/10.1016/j.jfoodeng.2012.02.016
Xanthopoulos, G. T., Templalexis, C. G., Aleiferis, N. P., & Lentzou, D. I. (2017). The contribution of transpiration and respiration in water loss of perishable agricultural products: The case of pears. *Biosystems Engineering, 158*, 76–85. https://doi.org/10.1016/j.biosystemseng.2017.03.011
Xin, Y., Liu, Z., Zhang, Y., Shi, X., Chen, F., & Liu, K. (2021). Effect of temperature fluctuation on colour change and softening of postharvest sweet cherry. *RSC Advances, 11*, 22969–22982. https://doi.org/10.1039/D1RA02610K
Xing, W., Liu, W., Li, H., Zeng, X., Fan, X., Xing, S., & Gong, H. (2025a). Development of predictive models for shelf-life of sweet cherry under different storage temperatures. *LWT, 217*, Article 117442. https://doi.org/10.1016/j.lwt.2025.117442
Xing, W., Liu, W., Li, H., Zeng, X., Fan, X., Xing, S., & Gong, H. (2025b). Development of predictive models for shelf-life of sweet cherry under different storage temperatures. *LWT, 217*, Article 117442. https://doi.org/10.1016/j.lwt.2025.117442
Zhang, Y., Zou, Y., Liu, L., Manzardo, A., Wang, X., & Wu, J. (2026). A digital twin–driven dynamic shelf life approach for mitigating food loss across fruit supply chains. *Journal of Stored Products Research, 117*, Article 103016. https://doi.org/10.1016/j.jspr.2026.103016
Zhu, Z., Chu, F., Dolgui, A., Chu, C., Zhou, W., & Piramuthu, S. (2018). Recent advances and opportunities in sustainable food supply chain: A model-oriented review. *International Journal of Production Research, 56*, 5700–5722. https://doi.org/10.1080/00207543.2018.1425014